Fluorescence-Based Methods for the Study of Protein-Protein Interactions Modulated by Ligand Binding

M.R. Stoneman[1], N. Raicu[1], G. Biener[1], and V. Raicu[1,2,*]

[1]Department of Physics, University of Wisconsin-Milwaukee, Milwaukee, Wisconsin, USA

[2]Department of Biological Sciences, University of Wisconsin-Milwaukee, Milwaukee, Wisconsin, USA

Abstract

Background: The growing evidence that G protein-coupled receptors (GPCRs) not only form oligomers, but that the oligomers also may modulate the receptor function provides a promising avenue in the area of drug design. Highly selective drugs targeting distinct oligomeric sub-states offer the potential to increase efficacy while reducing side effects. In this regard, determining the various oligomeric configurations and geometric sub-states of a membrane receptor is of utmost importance. *Methods:* In this report, we review two techniques which have proven to be valuable in monitoring the quaternary structure of proteins *in vivo*: Förster resonance energy transfer (FRET) spectrometry and fluorescence intensity fluctuation (FIF) spectrometry. In FRET spectrometry, distributions of pixel-level FRET efficiency are analyzed using theoretical models of various quaternary structures to determine the geometry and stoichiometry of protein oligomers. In FIF spectrometry, spatial fluctuations of fluorescent molecule intensities are analyzed to reveal quantitative information on the size and stability of protein oligomers. *Results:* We demonstrate application of these techniques to a number of different fluorescence-based studies of cells expressing fluorescently labeled membrane receptors, both in the presence and absence of various ligands. The results show the effectiveness of using FRET spectrometry to determine detailed information regarding the quaternary structure a receptor forms, as well as FIF and FRET for determining the relative abundance of different-sized oligomers when an equilibrium forms between such structures. *Conclusion:* FRET and FIF spectrometry are valuable techniques for characterizing membrane receptor oligomers which is of great benefit to structure-based drug design.

Keywords: FRET, fluorescence fluctuation spectroscopy, protein-protein interactions, FRET spectrometry, fluorescence imaging, ligand effect, oligomerization, quaternary structure

[*]Address correspondence to this author at the Department of Physics, University of Wisconsin-Milwaukee, Milwaukee, WI, USA; Tel: (1)4142294969; Email: vraicu@uwm.edu

1. INTRODUCTION

Intrinsic membrane proteins recognize and respond to a remarkable variety of stimuli that range from light to molecular ligands such as odorants, hormones, and neurotransmitters. The largest family of such proteins comprises the G protein-coupled receptors (GPCRs), which reside in the membranes of eukaryotic cells and initiate signal transduction processes by binding and activating a corresponding G protein residing within the cell [1-3]. GPCRs are of crucial physiological importance because of the wide range of functions they are involved in. They are also a prevalent target for the development of drugs due to the pivotal role they play in many diseases [4].

Interactions between GPCRs are known to play a vital role in a large number of biological processes [5, 6]. The growing realization that GPCRs may exist and function as oligomers [7-11] has profound implications for our understanding of GPCR-mediated signaling, and it raises many questions related to the oligomeric size, distribution within the cell, and functional role, as well as the effect of ligand-binding on oligomeric size and conformation [12, 13].

Quantification of the various oligomer configurations of a membrane receptor provides a promising avenue in the area of drug design. Designing a potential drug, most often a small ligand, involves modifying the molecule shape and charge to bind to the respective target and effectively activate or block its function [14, 15]. To this end, structural information regarding the biological target can greatly aid in the process of building potential ligands to most effectively bind and cause the highest amount of therapeutic response. However, when structural similarities exist across different receptors, difficulties arise as to the design of ligands which bind to a specific type of receptor but not to those with structural similarities. In this regard, quantification of the oligomerization of membrane receptors could provide a significant piece of information which could help elucidate a more pointed drug design strategy for a given receptor. It has been shown that some dimers exhibit different pharmacological responses than seen with their constituent monomers [16, 17], and compounds can be designed which specifically target a GPCR oligomer vs. the monomer alone [18, 19]. Consequently, drug discovery efforts which target oligomerized GPCRs, in contrast to ligands which aim to bind to receptors in the monomeric form, may help in identifying unique, and potentially desirable, pharmacological responses. It is also possible that receptors form higher order oligomeric states, and that the equilibrium between the different states is modulated by ligand binding [20].

Characterizing the quaternary structure of proteins in their native environment [21] is challenging, since many protein assemblies engage in dynamic association/disassociation equilibria, and thus they form a concentration-dependent mixture of different-sized oligomers, which complicates the determination of the quaternary structure. Therefore, methods are needed which permit determination of the local concentrations and spatial distributions of the differing possible types of oligomeric species (e.g., monomers, dimers, tetramers, etc.). Such techniques should allow the assessment of whether certain ligands may modulate the oligomeric size of the receptor or, conversely, whether the oligomeric size affects the binding efficiency of the ligand and thereby its potential efficacy as a drug. This would open up a new avenue of research in the area of cell signaling and would provide an untapped source of pharmacological targets.

In this report, we review two recently developed techniques which have proven to be valuable in quantifying protein interactions *in vivo*: Förster resonance energy transfer (FRET) spectrometry [22] and fluorescence intensity fluctuation (FIF) spectrometry [20]. In FRET spectrometry, pixel level distributions of FRET efficiency are analyzed using oligomeric models of various quaternary structures to determine the geometry and stoichiometry of protein oligomers. In FIF spectrometry, spatial fluctuations of protein molecules are analyzed with statistical methods to reveal quantitative information on the abundance of different-sized protein oligomers. The two techniques discussed in this review will potentially aid in drug research by elucidating the quaternary structure information of a biological target protein, allowing design of a drug that most effectively binds to that target and cause the desired therapeutic response.

2. FRET SPECTROMETRY

2.1. Overview of FRET

The mechanism of FRET occurs between two molecules which are separated by a short distance [23-25], at least one of which is fluorescent. One of the molecules (traditionally referred to as the donor molecule, D), brought into an

excited state by a light source, can transfer energy to a nearby molecule in the ground state (known as the acceptor molecule, A). The transfer of energy occurs non-radiatively, i.e., the donor does not emit a photon before returning to its ground state. The usefulness of FRET lies in the fact that this radiationless transfer of energy is highly distance-dependent and occurs when the two molecules are <10 nm from one another, which is conveniently on the same length scale as typical distances between individual protomers in protein complexes. By measuring and analyzing the efficiency with which this radiationless energy transfer occurs between proteins which are individually tagged with either a donor or acceptor molecule, information regarding the relative distance and orientation of the proteins with respect to one another can be extracted. The combination of FRET and fluorescence imaging has proved vital to the obtainment of quantitative information on protein-protein interactions [26-31], including size and structure of membrane receptor complexes [9, 10, 22, 32, 33], the spatial distribution of such complexes in living cells [34, 35], and the interaction energetics [27, 31, 36].

Standard FRET-based approaches for extracting detailed information about the interaction properties of a given protein typically rely on measuring the average FRET efficiency, E_{ave}, computed over large regions within a cell or multiple cells, as a function of the D and/or A relative abundances within those regions. We refer to this dataset as an abundance spectrum of E_{ave}. The independent variable in an abundance spectrum of E_{ave} may be either the ratio of the donor to acceptor concentrations in the sample [37] (or, equivalently, the mole fraction of donors or acceptors [38-40]), or the total concentration of donors plus acceptors [30, 41, 42]. Regardless of its specific form, the value of the abundance spectrum is that the concentration of oligomers can be determined by fitting to it a model that is derived from the kinetic theory of FRET [43] and that uses the concentration of oligomers as a fitting parameter. The process of extracting the concentration of oligomers from an abundance spectrum can then be repeated for a range of different receptor concentrations in order to determine the association/dissociation constant describing the strength of interactions between proteins in the oligomer. Unfortunately, these methods only work well if you know either the composition of the sample with respect to the different-sized oligomer species (i.e., number of monomers, dimers, higher order oligomers) or the FRET efficiency occurring between one of the donor/acceptor pairs in the protein complex (i.e., the pairwise FRET efficiency, E_p [43]), since a vast number of combinations between sample composition and E_p values fit the data equally well.

The recently developed method of FRET spectrometry has been designed specifically to determine the quaternary structure of a protein complex and thereby reveal detailed information about the structure, such as the value of E_p [9, 22, 32, 44]. In FRET spectrometry, a value of FRET efficiency is calculated for every pixel in a fluorescence image. Because the molecular complexes within a given pixel may consist of a mixture of several different combinations of donors and acceptors, we refer to this pixel-level value of FRET efficiency as the apparent FRET efficiency, E_{app}, because it is the average FRET efficiency per donor molecule residing within a given pixel. Distributions of E_{app} values, as opposed to averages over large regions, are modeled using theoretically predicted values of FRET occurring in protein complexes [43] which possess a particular size and geometry. The model that produces the best agreement with the experimentally measured E_{app} distributions is taken as the quaternary structure of the protein. The detailed geometrical parameters associated with the determined quaternary structure model can then be combined with an abundance spectrum of E_{ave} to obtain the relative proportions of various oligomer species comprising the sample [38]. The combination of these two FRET approaches is vital, e.g., when ligand binding to a receptor leads to changes in both the oligomer conformation and the proportion of different oligomeric sizes (e.g., dimers and tetramers), which is often the case with biologically-relevant oligomers [45-47].

2.2. FRET efficiency in multimeric complexes

In FRET spectrometry, E_{app} distributions are simulated using theoretical models of the FRET occurring in oligomer complexes in order to determine the quaternary structure of the protein. The measured distributions of FRET efficiency, also referred to as FRET spectra or spectrograms, provide a unique "fingerprint" corresponding to a particular quaternary structure of a protein complex. This feature stems from the fact that there exist a number of different ways in which donors and acceptors may be placed at the various protomer locations within the oligomer. Each of these different ways, or "configurations", can exhibit a different FRET efficiency value, depending on both the number and placement of the donors and acceptors in the particular configuration. The collection of different FRET efficiency values exhibited by different oligomer configurations show up as peaks in the measured E_{app}

distributions. The number of peaks and spacing between them uniquely corresponds to a particular oligomer size and geometry. The measured FRET spectrogram can be fitted with theoretically predicted FRET efficiencies, which are generated using the kinetic theory of FRET in multimeric complexes of donors and acceptors [43], to find the oligomer size and geometry which best simulate the measured FRET efficiency distribution. The theoretical treatment of FRET in multimeric complexes is briefly outlined below; for more extensive reviews of this theory, please see references [22, 48].

Each donor molecule in an oligomeric complex which contains a total of *k* donors and *n-k* acceptors may lose excitation energy through a number of different pathways. One de-excitation pathway results in radiative emission of a photon, one corresponds to a non-radiative de-excitation of the donor via interactions with the environment, and *n-k* pathways result in a transfer of excitation energy via FRET to one of the *n-k* nearby acceptors. The probability of energy transfer to one of the nearby *n-k* acceptors depends on the acceptor distance and orientation relative to the donor. The total efficiency of energy transfer occurring for a single donor, *i*, in a complex of size *n*, number of donors *k*, and configuration *q*, is given as follows [32, 43, 48]:

$$E_{i,k,q} = \frac{E_p \sum_j \left(\frac{r_1}{r_{ij}}\right)^6}{1 - E_p + E_p \left[\sum_j \left(\frac{r_1}{r_{ij}}\right)^6\right]}. \quad (1)$$

where, $r_{i,j}$ represents the distance between the i^{th} donor and j^{th} acceptor. The sum over *j* in eq. (1) represents all acceptors in close proximity to the donor, i.e., the sum is over all *n-k* acceptors within the same complex. Implicit in eq. (1) is the assumption that only one donor in a complex is brought into an excited state at a time. This is achieved by keeping the excitation light power low enough so that the donor excitation rate is much lower than the radiative decay rate. The pairwise FRET efficiency, E_p, represents the FRET efficiency occurring between a single donor and acceptor separated by a distance corresponding to one of the side lengths, r_1, in the oligomer complex (see Fig. **1A**), and is given as follows:

$$E_p = \frac{\left(\frac{R_0}{r_1}\right)^6}{1 + \left(\frac{R_0}{r_1}\right)^6}. \quad (2)$$

where R_0 is the Förster radius [25], which equals the distance at which the efficiency of energy transfer between the two fluorophores is 50%. Since all donors in a complex of configuration *q* emit signal from the same sample voxel (or image pixel), pixel-level measurements do not discriminate between signals from individual donors, and they therefore provide an average efficiency per donor:

$$E_{k,q} = \frac{1}{k} \sum_{i=1}^{k} E_{i,k,q}. \quad (3)$$

Eqs. (1) and (3) provide a means to compute expressions for the FRET efficiencies of various configurations of donors and acceptors within an oligomeric complex of a certain size and geometry. An example of the computed $E_{k,q}$ values for each possible configuration of a particular tetramer oligomer shape are listed in Fig. **1B**.

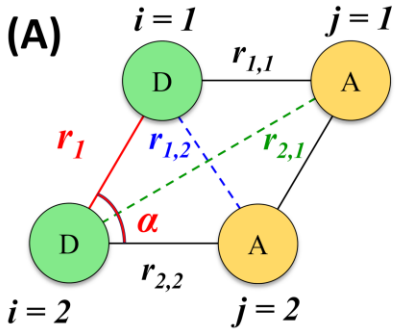

(B)

	k	q	$E_{k,q}$
	4	1	0
	3	1	0.345
	3	2	0.345
	3	3	0.500
	3	4	0.500
	2	1	0.588
	2	2	0.588
	2	3	0.588
	2	4	0.588
	2	5	0.667
	2	6	0.667
	1	1	0.671
	1	2	0.671
	1	3	0.750
	1	4	0.750
	0	1	0

Fig (1). (A) Illustration showing a single configuration of a rhombus-shaped tetramer ($n = 4$) with $k = 2$ donors (green circles) and (n-k) = 2 acceptors (yellow circles). For the specific case of the rhombus, the various r_{ij} distances can all be computed from two parameters, r_1 and α, which are highlighted in red. $r_{1,1} = r_1$, $r_{2,2} = r_1$, $r_{1,2} = 2r_1\, cos\left(\frac{\alpha}{2}\right)$, and $r_{1,2} = 2r_1\, sin\left(\frac{\alpha}{2}\right)$ **(B)** Table listing each possible configuration and corresponding $E_{k,q}$ value of a rhombus shaped tetramer. To calculate $E_{k,q}$, the acute angle of the rhombus was set to be equal to 60° and $E_p = 0.5$; this particular value of E_p occurs when the side length of the rhombus, r_1, is equal to the Forster radius, R_0, of the two fluorophores. The rows of the table are color coded to group together configurations with approximately equivalent $E_{k,q}$ values; these values form the primary peaks in the meta-histogram.

2.3. Pixel-level calculation of FRET efficiency from intensity-based measurements

While a number of fluorescence imaging methods can be used to measure the FRET efficiency occuring in a sample of interest, FRET spectrometry currently utilizes intensity-based sensitized emission. For intensity-based measurements, laser scanning microscopes which employ spectral resolution [49-54] are ideal, because they allow for the quantitation of both donor and acceptor fluorescence intensity, from which the FRET efficiency can be straightforwardly calculated. The acquisition of an entire fluorescence spectrum enables overlapping spectral profiles to be separated by capitalizing on the distinct shapes of the elementary spectra comprising the composite fluorescence spectrum using spectral unmixing [10, 37, 55-57]. By applying spectral unmixing to the measured composite fluorescence spectrum for each image pixel, 2D maps of donor intensity in the presence of the acceptor, k^{DA}, and acceptor intensity in the presence of the donor, k^{AD}, which represent the coefficients multiplying each elementary spectrum composing the theoretical curve fitting the measured composite spectrum, can be extracted. Multiplying the k^{DA} and k^{AD} values with the area underneath their respective elementary spectrum gives the total fluorescence intensity of the donor, $F^{Da} = k^{Da}w^D$, and acceptor, $F^{Ad} = k^{Ad}w^A$, detected for each individual pixel. The values of w^D and w^A represent the areas under the donor and acceptor emission spectra, respectively. The apparent FRET efficiency, E_{app}, is calculated from the measured intensity values according to the following:

$$E_{app} = 1 - \frac{F^{Da}}{F^{D}} \tag{4}$$

Here, F^D represents the fluorescence of the donor in the scenario where there is no acceptor present. Of course, a single fluorescence measurement which quantifies donor and acceptor fluorescence is not generally enough to determine the value of F^D. However, if an excitation wavelength is chosen such that there is no direct excitation of the acceptor, then eq. (4) can be simplified to give [10]:

$$E_{app} = \frac{F^{Ad}}{\frac{Q_A}{Q_D} \cdot F^{Da} + F^{Ad}} \tag{5}$$

Eq. (5) can be used to determine the FRET efficiency at each pixel in a spectrally resolved fluorescence microscope following a single scan of the sample at a single excitation wavelength, assuming minimal direct excitation of the acceptor occurred. However, if no assumption regarding the direct excitation of the acceptor can be made, a second scan of the sample at a second excitation wavelength can be executed to acquire two more measured quantities, i.e., the fluorescence of the donor and the fluorescence of the acceptor at the second excitation wavelength, F_2^{Da} and F_2^{Ad}, respectively. By incorporating the scan of the sample at the second excitation wavelength, the apparent FRET efficiency can now be written entirely as a function of measurable quantities [42]:

$$E_{app} = \left[1 + \frac{F_1^{Da}\left(1 - \rho^{ex,A}/\rho^{ex,D}\right)}{F_1^{Ad} - F_2^{Ad}\rho^{ex,A}} \frac{Q^A}{Q^D} \right]^{-1} \tag{6}$$

where the indices 1 and 2 denote measurements performed using the first and second excitation wavelength, respectively. Values for $\rho^{ex,D} = \frac{F_1^D}{F_2^D}$ and $\rho^{ex,A} = \frac{F_1^A}{F_2^A}$ can be found by measuring a sample expressing only the donor or only the acceptor, respectively, at the two excitation wavelengths. Using eq. (6), or eq. (5) if direct excitation of the acceptor is minimized, the apparent FRET efficiency can be calculated for each pixel in a spectrally resolved fluorescence image.

2.4. Extraction of quaternary structure from fitting of "meta-histogram"

The quaternary structure of a protein of interest can be determined by modeling a collection of FRET spectrograms with the FRET efficiency values expected from an oligomeric structure with a particular size and shape, i.e., the $E_{k,q}$ values predicted by eq. (3) in section 2.2. As can be seen via the color coding of different rows in Fig. **1B**, there are degenerate FRET efficiency levels, or, in other words, there are FRET values which correspond to more than one configuration of a particular oligomer model. The location and number of peaks visible in a FRET spectrum can be correlated to the value and number of degenerate FRET efficiency levels occurring for a given oligomer size and shape. The number of degenerates, and hence number of visible peaks, depends on the size and shape of the oligomer complex. For example, in the case of the rhombus-shaped tetramer of Fig. **1A**, there are five unique FRET efficiency values. Successful correlation of the peaks of the FRET spectrum to a set of predicted FRET levels resolves the size and structure of the protein complex under study.

However, if pixels within the measurement contain several different oligomer configurations with different $E_{k,q}$ values, and/or are mixed with monomers or other oligomeric species, the measured apparent FRET efficiency for the given pixel will reflect an average over the entire population of complexes within the pixel. These mixtures broaden the distribution of E_{app} values such that it becomes difficult to identify the unique "fingerprint" of the underlying oligomer complex. Therefore, in order to accentuate the peaks occurring due to the degenerate $E_{k,q}$ values, a large number of E_{app} values must be sampled and further distilled. The distilling of the apparent FRET efficiency values is accomplished by the generation of a "meta-histogram" [22, 32, 38, 44, 58], which is described in more detail in the following paragraphs.

The process of generating a meta-histogram begins by demarcating small segments (~100 pixels^2) on the fluorescence images which enclose pixels where the protein of interest is located. Typically, 2-6 segments are demarcated for each cell scanned, depending on the cell size. The FRET efficiency values from each of the pixels falling within a segment are then organized into a histogram plot, or FRET spectrogram, of bin width equal to 0.005.

Fluorescence images from a large number of cells need to be collected such that the total number of segments, and hence number of FRET spectrograms, is greater than 1000. To collectively analyze all of the information contained within the set of spectrograms, the positions of only the most prominent peaks in each individual histogram are recorded. The collected peak values are then used to generate a plot consisting of the number of peaks that fall in a certain interval of E_{app} values against the center of the E_{app} interval, a plot which has been termed a meta-histogram. In order to select the most prominent peak positions from individual FRET spectrograms, an automated algorithm is employed where only peaks with amplitudes which pass a particular selection criterion are chosen. This selection criterion ensures that peaks appearing simply due to random fluctuations are disregarded. Modeling the location of the peaks within the meta-histogram is the essence of the FRET spectrometry approach, and, therefore, the bin sizes used for generating the individual E_{app} histograms (0.005) as well as the meta-histogram (0.02) have been specifically chosen such that closely spaced peaks are still distinguishable in the meta-histogram, while avoiding aliasing effects, which can generate "false peaks".

The generation of the meta-histogram, as opposed to simply summing up all the individual E_{app} histograms, effectively filters out E_{app} values that arise due to combinations of oligomers with different donor and acceptor configurations. An additional advantage of the meta-histogram is that receptor complexes associate and dissociate within a time shorter than the time needed to acquire an image of an entire cell, which leads to oligomers with similar size and proportion of D and A throughout the cell membrane. This effect generates single narrow peaks in the individual FRET spectrograms and does not illustrate the complete array of oligomer sizes and D-A combinations; the meta-histogram takes all such combinations into account.

In order to find the oligomeric structure model which best fits the data, the meta-histogram is simulated with a theoretical fitting function consisting of a sum of Gaussian functions, with the mean of each Gaussian corresponding to the $E_{k,q}$ values predicted for the various configurations of a particular oligomer model, and the total number of Gaussians corresponding to the number of unique $E_{k,q}$ values predicted for the given model. The fitting function is given as follows:

$$ModelFunction(E_{app}) = \sum_l A_l exp\left[-\frac{(E_{app}-E^l)^2}{2\sigma_l^2}\right] \quad (7)$$

where A_l, E^l, and σ_l represent the amplitude, mean, and standard deviation of the l^{th} Gaussian distribution. The meta-histogram is fit with various oligomeric size and structure model functions, and the model attaining the best fit between the meta-histogram and the model function is chosen. The fitting of the theoretical models to the experimental data is achieved by a minimization of a reduced fitting residual:

$$Res = \sqrt{\sum[Data - ModelFunction]^2}/f, \quad (8)$$

where f is the number of degrees of freedom, defined as the number of data points minus the total number of adjustable parameters minus 1.

For each meta-histogram fitting, the amplitudes and standard deviations of each Gaussian in the model function are allowed to vary. The centers of each Gaussian, which correspond to the different degenerate FRET efficiency levels, are linked through the pairwise FRET efficiency, E_p, as well as other geometrical parameters specific to the particular oligomer model being tested. For example, for the case of the rhombus-shaped tetramer in Fig. **1A**, the relationship between the various FRET values are all determined solely through E_p and the angle between the sides of the rhombus, α. Therefore, the only fitting parameters allowed to vary regarding the means of the Gaussians would be E_p and α. A total of five Gaussians would be needed to simulate the rhombus-shaped tetramer, as is illustrated with the color-coding of the unique values of $E_{k,q}$ in Fig. **1B**. For more complicated geometries, additional geometrical parameters, e.g., ratio between the lengths of the sides, also need to be included to completely determine the set of FRET efficiency values, and therefore are needed as adjustable parameters in the fitting process.

2.5. Computer program for meta-histogram analysis

A user-friendly software package for simulating meta-histograms with a parallelogram shaped tetramer oligomer has been developed and can be downloaded from the following link (https://figshare.com/s/d56b6b8678e2f41db6d6).

Meta-histograms can be loaded into the program by formatting the data as a two column tab-delimited text file containing the E_{app} bin interval centers in the first column and the corresponding number of peak positions obtained for each E_{app} interval in the second column. The points in the experimental meta-histogram are displayed as blue circles in the main plotting window, which is bordered by the blue rectangle in Fig. **2**. Also plotted in the same window as the measured meta-histogram is a function consisting of a sum of Gaussians. The positions of all the Gaussian means are completely determined by three geometric variables, i.e., E_p , α, and r_1/r_2, which define the shape of a parallelogram-shaped oligomer. Finally, two vertical colored lines are also displayed in the main plotting window. The blue and red vertical lines indicate the FRET efficiency location of two different donor/acceptor dimers which could form as a result of the tetramer splitting along either the horizontal (red line) or vertical (blue line) axis. An illustration of the two types of dimers is shown in the Tetramer Splitting Into Dimers panel of Fig. **2.** The locations of the vertical lines serve as a guide for assessing whether the sample was comprised of dimers and tetramers in equilibrium, as the presence of either one of the dimers would show up in the meta-histogram as an additional peak, or an enhancement of one of the tetramer peaks, at the location of the corresponding vertical line.

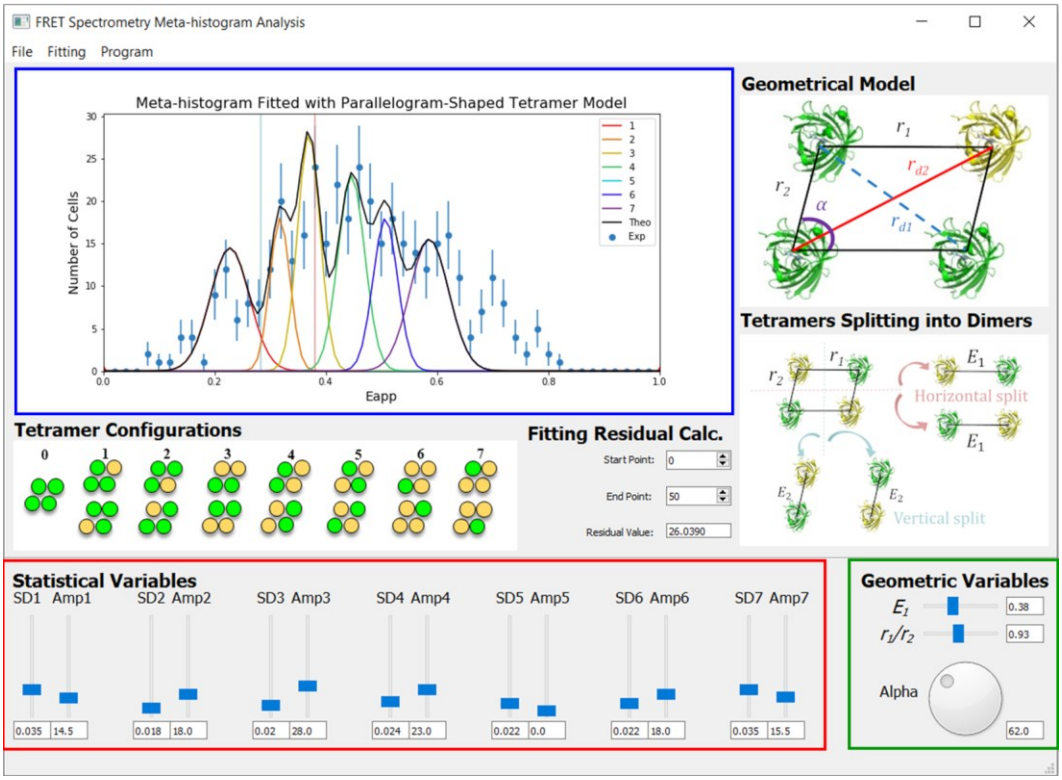

Fig. (2). Graphical user interface of the program used to extract the quaternary structure of a protein complex from meta-histograms**.** Measured meta-histograms are plotted in the main plotting window (enclosed by the blue rectangle); the data are represented by solid blue circles. The solid black line represents a sum of Gaussians with each individual Gaussian (represented by solid lines of various colors) corresponding to the $E_{k,q}$ values of different configurations of the parallelogram-shaped tetramer model, which is pictured in the **Geometrical Model** window in the upper right hand corner. The positions of all the Gaussian peaks are completely determined by three geometric variables which define the size and shape of the parallelogram, i.e., E_p , α, and $^{r_1}/_{r_2}$; these three parameters can be adjusted by the slider bars and the dial in the **Geometric Variables** panel (enclosed by the green rectangle). Finally, the amplitude (Amp) and standard deviation (SD) of each individual Gaussian can be adjusted by the corresponding slider bar in the **Statistical Variables** section (enclosed by the red rectangle). The simulated curve updates in real time when any of the controls for statistical or geometric variables are adjusted. This program is available for use and can be downloaded from the following link (https://figshare.com/s/d56b6b8678e2f41db6d6).

The values for the three geometrical parameters describing the model are controlled via slider bars and dials on the program GUI, as indicated in the Geometric Variables panel of Fig. **2**. Modifying these geometrical parameters

will update the Gaussian peak positions of the simulating function. The amplitudes and standard deviations of the various Gaussian functions can also be controlled from the program GUI. The user first achieves a "rough fit" of the meta-histogram by manually adjusting the geometrical parameters of the model as well as the amplitude and standard deviation of each of the assigned Gaussians. Once an approximate fit is achieved, an automated minimization algorithm can be applied to fine-tune the fitting. The reason the fitting is first attempted manually by the user is because the fitting parameter space is quite large, and the minimization algorithm applied by itself is susceptible to falling into a local minimum. Future updates to the program will include more flexibility with regard to the geometrical model chosen, including the option for choosing different oligomer sizes and shapes.

2.6. Effect of ligand binding on the quaternary structure of sigma-1 receptors

The method of FRET Spectrometry was applied to fluorescence images acquired of COS-7 cells expressing the sigma-1 receptor (S1R) in order to gauge the effect of various ligands on the quaternary organization of S1R [58]. S1R is a transmembrane chaperone protein primarily found in the endoplasmic reticulum, but, upon stimulation with agonist, S1R can translocate to the plasma membrane to interact with ion channels and other receptors, including GPCRs. S1R is regulated by various synthetic molecules acting as either agonists, e.g., pentazocine, or antagonists, e.g., haloperidol.

Meta-histograms for S1R-expressing cells are shown in Fig. **3** for unliganded (Fig. **3A**), pentazocine-treated (Fig. **3B**), and haloperidol-treated cells (Fig. **3C**). The meta-histograms, which present several uniformly spaced peaks, were found to be best fitted with a model incorporating a mixture of monomers and dimers. In this model, the number of predicted peaks in the meta-histogram scales linearly with the average number of donors present in a given pixel. Therefore, only regions in the cell with low expression levels can be properly analyzed; when too many peaks are present, the amount of overlap between them causes the meta-histogram to lose the identifying features needed to resolve the oligomeric structure. An illustration of the various combinations of monomers and dimers, along with the corresponding E_{app} values which give rise to the various peaks in the meta-histogram are shown in Fig. **4D**. The best fit value for the pairwise FRET efficiency of the donor-acceptor dimer was found to be E_p=0.433 for the unliganded cells; this value did not change significantly when the cells were treated with either pentazocine (E_p=0.435) or haloperidol (E_p=0.435).

Upon inspection of the FRET spectrograms obtained from individual S1R-expressing cells, it was found that a number of cells with higher expression levels exhibited apparent FRET efficiency values larger than the pairwise FRET efficiency value, E_p=0.435, extracted from the meta-histogram fitting. This finding indicated the presence of higher order oligomers present in some of the cells, as the highest FRET efficiency value attained in a mixture of only monomers and dimers is the pairwise FRET efficiency of the donor-acceptor pair, E_p (see Fig. **4D**). Therefore, in order to gauge the S1R interaction properties at higher receptor concentrations, averages of E_{app} were determined for entire cells and plotted against the average number of donor-tagged receptors within the corresponding cell. By qualitatively examining the behavior of cellular averages of E_{app} at the lower and higher end of the measured concentration range, information on the smallest and largest oligomeric structure in the system could be ascertained. At the lower end of the concentration range, E_{app} values were never higher than E_p, suggesting that the largest oligomer structure in this concentration range was a dimer; this was true for all samples investigated. However, at the higher end of the donor concentration range, E_{app} values were more broadly distributed and exceeded the value of E_p in a number of the samples, indicating that S1R most likely formed dimers as well as higher order oligomers. Specifically, the results indicated that in untreated cells, S1R was present in monomeric, dimeric, and even higher order oligomeric forms. Addition of haloperidol stabilized the S1R in the higher oligomeric state, as higher values and a larger spread in E_{app} values was observed in these cells compared with the untreated ones. Pentazocine had the opposite effect, as the highest attained value of E_{app} was E_p, indicating that Pentazocine stabilized the dimer formation and prevented formation of higher order oligomers.

A number of key takeaways can be made from the results of the FRET based study of S1R: (i) using FRET spectrometry, it was found that the most prevalent oligomeric structure formed by S1R was dimeric in form, and that the relative distances between protomers within this dimer remained unchanged after ligand binding. (ii) A combination of this structural information with observations gleaned from a qualitative introspection of FRET efficiency values obtained from averages over entire cells proved quite valuable, as it gave insight into the relative

proportion of monomers and different-sized oligomeric species comprising the system as a function of treatment with various ligands. The latter takeaway led to the development of a more rigorous combination of FRET spectrometry with average-based approaches, the likes of which will be discussed in the next section.

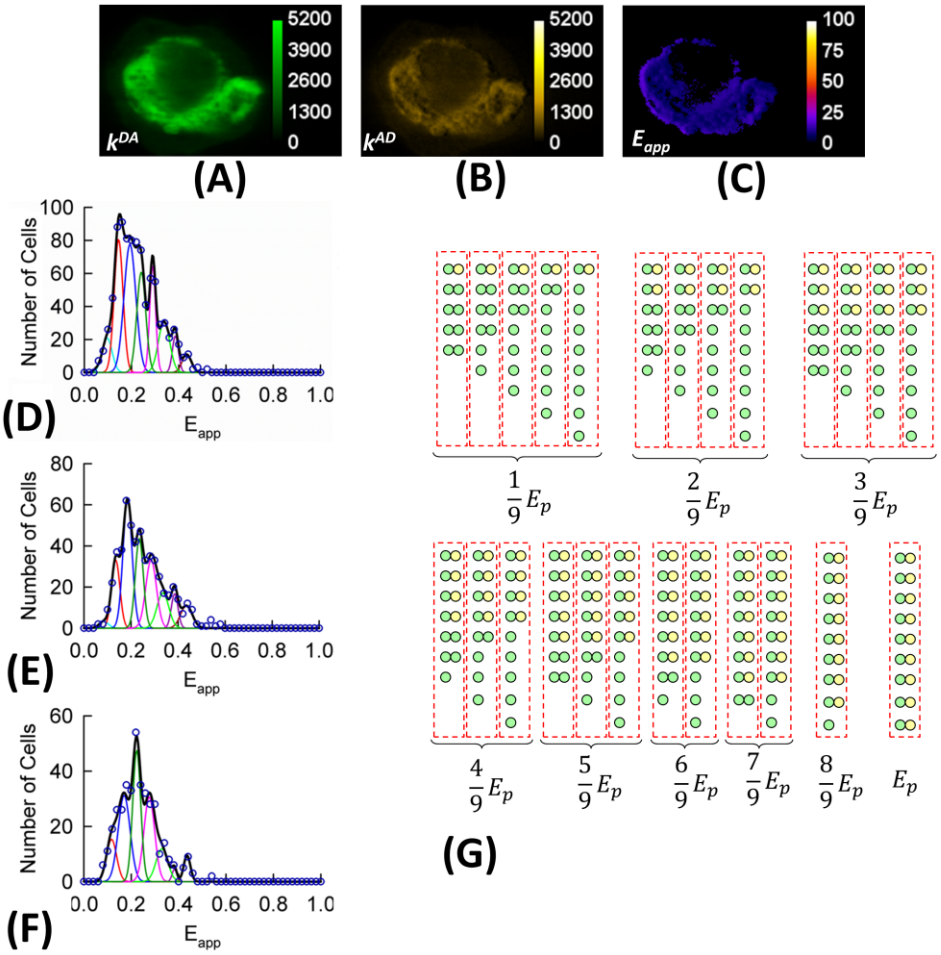

Fig. (3). FRET spectrometry results obtained from COS-7 cells expressing sigma-1 receptors labeled with one of GFP2 or YFP in the absence of ligand (-L) or in the presence of either an S1R agonist (pentazocine) or antagonist (haloperidol). Figure was adapted from Mishra *et al.* in Biochemical Journal 2015 [58]. **(A-C)** Representative two-dimensional maps of the (A) fluorescence of donors in the presence of acceptors (k^{DA}) and (B) acceptors in the presence of donors (k^{AD}). The two-dimensional maps of k^{DA} and k^{AD} were used to compute the (C) apparent FRET efficiency (E_{app}) for each pixel according to eq. (5). **(D-F)** Experimentally determined meta-histograms (blue circles) obtained from COS-7 cells expressing S1R receptors which were (D) unliganded, (E) treated with haloperidol (antagonist), and (F) treated with pentazocine (agonist). Each meta-histogram was simulated (solid black line) using correlated Gaussian functions (shown individually with various colored lines) and as a sum (thick black line). The centers of each of the Gaussians was predicted by the theoretical model consisting of dimers and monomers, which is illustrated in (G). The best-fit value for the pairwise FRET efficiency for each of the samples was: (D) E_p=0.433 (E) E_p=0.435 and (F) E_p=0.435 **(G)** Geometrical configurations and corresponding E_{app} values for mixtures of dimers and donors. Donor and acceptor molecules are shown by green and yellow circles, respectively. A number of different combinations of donors and dimers can give rise to the same E_{app} value; each such individual combination is bordered by a red-dashed rectangle. Combinations which give rise to the same E_{app} value are grouped together by braces, with their corresponding E_{app} value underneath the brace. The number of predicted E_{app} values increases proportionally with the average number of donors. Each of the meta-histogramss in (D-F) was fit with a sum of nine Gaussian functions.

2.7. Combined analysis of FRET spectrograms and abundance spectra of E_{ave}

A combination of the FRET spectrometry approach with analysis of the abundance spectrum of average FRET efficiencies has led to the determination of the relative proportion of oligomers formed by two different GPCRs, i.e., opsin [32] and the sterile 2 alpha factor receptor (ste2) [38]. Combining the two approaches capitalizes on the capability of FRET spectrometry in determining the dominant quaternary structure, and thereby the relevant geometrical parameters, of the protein of interest. The geometrical parameters obtained from fitting of the meta-histogram in FRET spectrometry are input and fixed when fitting the abundance spectrum of the average FRET efficiency, a procedure which is briefly described below.

An average value of FRET efficiency, E_{ave}, is determined for each segment (see Section 2.4 for definition of segment) by inserting average values of F^{Da} and F^{Ad}, computed over all the pixels in the segment, into eq. (5). Likewise, in the same segment, the average F^{Da} and F^{Ad} values are used to calculate the average concentration of both donors and acceptors [38] in the segment. The donor and acceptor concentration values are then used to calculate the fraction of total fluorophores which are acceptors, X_A, for the given segment. A plot of E_{ave} vs X_A is then constructed and simulated with a model predicting the FRET efficiency of a mixture of various sized oligomers, given by the following [43]:

$$E_{app,theo} = \frac{1}{\sum_n N_{D,n}} \sum_n N_{D,n} E_{app,n}, \tag{9}$$

Here, $E_{app,n}$ is the apparent FRET efficiency for a population of oligomeric complexes in which each complex has the same shape and size (n), given by:

$$E_{app,n}(X_A) = \frac{1}{n(1-X_A)} \sum_{k=1}^{n-1} \sum_{q=1}^{\binom{n}{k}} (1-X_A)^k \, X_A^{n-k} k E_{k,q}, \tag{10}$$

where $[n(1-X_A)]^{-1}$ is the average number of donors within a complex when averaged over all configurations the complex can take. Because $E_{app,n}$ is defined as the energy transfer per donor in a complex of size n, each term in the summation of eq. (9) is weighted with the total number of donors participating in complexes of size n:

$$N_{D,n} = n\mu_n(1-X_A). \tag{11}$$

where μ_n is the total number of oligomers of size n within the mixture.

By fitting plots of E_{ave} vs. X_A with eq. (9), and fixing the various $E_{k,q}$ terms at values which were pre-determined from the analysis of the meta-histograms, the only free parameters left for adjustment are the abundance of each of the different sized species, μ_n, which can be extracted by achieving the best fit between eq. (9) and the data. Furthermore, by applying this fitting to E_{ave} vs. X_A curves constructed from a number of different concentration ranges, and thereby obtaining μ_n values for each such range, the dissociation constant for the particular structure may also be determined.

Using this combined FRET spectrometry and abundance spectra of E_{ave} approach, it was determined that opsin receptors expressed in Chinese hamster ovary (CHO) cells formed an equilibrium of dimers and tetramers at low concentration levels, and the ratio between the two, μ_4/μ_2, increased with increasing concentration. By, fitting the dependence of μ_4/μ_2 with a model derived form the Law of Mass Action, it was found that the dissociation constant of the tetramer-to-dimer equilibrium was 87 molecules/μm^2 [32]. As the concentration increased even further, the model used to fit the meta-histogram and E_{ave} vs. X_A curves needed to incorporate octamers into the mixture of oligomeric complexes. In a separate study, yeast cells expressing fluorescently labeled ste2 formed primarily tetramers at the lowest measured concentration range ($\mu_4/\mu_2 > 1000$). At higher concentrations, higher order oligomers started to appear, as the E_{ave} vs. X_A curves were best fit with a mixture of tetramers and octamers ($\mu_8/\mu_4 = 1.38$) [38].

As is evident from the preceding sections, FRET spectrometry provides a powerful means for gleaning the size and structure of the most dominant oligomer structure formed by fluoresecntly labeled membrane receptors. The main challenge in the FRET spectrometry approach is that it necessitates the implementation of a rather complicated analysis procedure due to the requirement that the fluorescence data must be acquired at relatively low protein

concentrations (< 25 molecules/pixel). At higher concentrations of molecules, mixtures of various possible configurations of an oligomer complex in a pixel removes the unique features present in the measured FRET spectrograms needed to identify the oligomer geometry. When this is the case, an alternative fluorescence-based method, which we describe in the subsequent section, may be used to obtain information regarding the average size and abundance of various oligomers in the sample.

3. 2D FIF SPECTROMETRY

3.1. Overview of fluorescence fluctuation spectroscopy (FFS)-based methods

In FFS-based approaches, fluorescence intensity fluctuations occurring due to fluorescently labeled molecules diffusing in and out of a microscope focal region are analyzed with various statistical methods to reveal properties of the molecules, such as the diffusion coefficient or aggregation state. Originally applied to quantify the diffusion of fluorescently labeled molecules in solution by analyzing the correlations between the intensity fluctuations, FFS-based approaches have been extended in recent decades to allow quantification of the abundance and interactions of the molecules, not only in solutions, but in living cells as well. The subset of FFS techniques which specialize in quantifying the abundance and interaction of biomolecules, such as Photon-Counting Histogram (PCH) analysis [59, 60], Number and Brightness (N&B) analysis [61-63], and Spatial Intensity Distribution Analysis (SpIDA) [47, 64], rely on analyzing the moments of fluorescence intensity distributions obtained from the fluorescently labeled molecules. The crux of all the moment-based techniques is the relation between the molecular brightness, defined as the average detected signal of a single fluorescent molecule over a given time period, and the amplitude of the intensity fluctuations. To better understand this relationship between the molecular brightness and intensity fluctuations, picture a dimeric complex comprised of two identical fluorescent molecules diffusing in and out of the excitation volume of a laser scanning microscope. Movement of the dimeric complex through the focal region will cause a larger fluctuation in fluorescence signal than a monomer of the same fluorescent protein, simply due to the fact that there are twice as many fluorophores in the dimer compared to the monomer.

The molecular brightness of a complex of fluorescently labeled proteins scales linearly with the size of the complex, e.g. a dimer has twice the molecular brightness of a monomer. Therefore, the set of moment-based FFS techniques, which extract the molecular brightness from distributions of fluorescence intensity, have been shown to be very effective for determining the size at which a protein complex forms [64-67]. However, when the relative proportion of the various states of a particular protein varies, e.g. as a function of concentration, these traditional FFS-based approaches only provide average values of the oligomer size over the entire concentration range, and therefore may give different results on the stoichiometry of the protein complex which depends on the expression level of the sample.

A recently developed moment-based technique, termed Two-Dimensional Fluorescence Intensity Fluctuation (2D FIF) Spectrometry [20], provides quantitative information on the size and stability of protein oligomers as a function of receptor concentration using intensity fluctuations resulting from variations in the molecular concentrations from pixel to pixel. In FIF spectrometry, molecular brightness values are calculated from small groups of pixels, or segments, and compiled into a distribution. Analysis of the brightness distributions, or spectrograms as they have been termed, as opposed to averaging brightness values over large regions, is advantageous in that the spectrograms preserve information regarding fluctuations in oligomer size occurring across the membrane. The brightness spectrograms can be unmixed, based on knowledge of a monomeric brightness spectrogram, to obtain the relative contribution of the different sized oligomeric species. A second advancement in 2D FIF is the extraction of individual protomer concentrations within an ensemble of oligomers. This allows the sorting of molecular brightness spectrograms as a function of concentration, enabling the generation of oligomerization kinetics curves, represented by the relative abundance of the monomers and various-sized oligomers comprising the sample as a function of the total concentration of molecules.

The 2D-FIF approach may be implemented using standard laser scanning fluorescence microscopes. The only requirement is that the pixel dwell time be at least a factor of five times shorter than the characteristic diffusion time, τ_D, of the receptor under study. The characteristic diffusion time is the average time a receptor molecule will reside within the measurement volume before diffusing out and is related to the laser beam waist, ω_o, the diffusion

coefficient, D, and the dimensionality of the diffusion, *d,* through the following relation $\tau_D = \frac{\omega_o^2}{2dD}$. The laser beam waist is defined as the distance from the center of the focused beam to the location where the intensity of the beam drops to e^{-2} its maximum value. If the pixel dwell time is too long in comparison to the characteristic diffusion time of the molecule, then the fluctuations in number of molecules, and thereby fluorescence intensity, occurring from pixel to pixel will be averaged out due to molecules diffusing through the measuring volume within the span of a single measurement.

In the following sections, we will describe in more detail the FIF spectrometry approach and specify how it is used to discern the oligomerization kinetics of the human secretin receptor (hSecR) as well as assess the effect on the oligomerization properties induced by exposure of the receptors to their endogenous ligands (secretin).

3.2. Calculation of molecular brightness and concentration for each image segment

The 2D-FIF spectrometry method relies on collecting fluorescence images of cells expressing the receptor of choice fused to a fluorescence marker protein. Large regions of interest are drawn on individual cells in the fluorescence images and divided into smaller subregions, or segments, typically on the order of ~400 pixels^2. A fluorescence intensity distribution is generated for each segment, from which the average, $\langle I_s \rangle$, and variance of the distribution, σ^2, are computed by fitting the distribution with a single Gaussian function. The extracted average and variance of the intensity distribution is then used to calculate an "effective molecular brightness," ε_{eff}, for the segment. Finally, the average intensity of the segment is divided by the effective molecular brightness of a single protomer, $\varepsilon_{eff}^{proto}$, to determine the average concentration of receptors in that segment.

The purpose of segmenting the large ROI into smaller segments is twofold: (i) calculating brightness and concentration from large pixel areas has the effect of averaging out fluctuations of concentration and oligomer size which may be occurring across the ROI, because only a single brightness value is obtained for each pixel area. (ii) segmentation effectively separates regions in the cell containing small groups of pixels, or "spots", which contain a significantly higher average intensity than the pixels in their neighboring regions. Molecular brightness values calculated for these segments which contain high intensity spots skew very highly with respect to the distribution of brightness values constructed from all segments. However, the 2D FIF approach of deconvoluting such brightness distributions, detailed in section 3.3, naturally filters out these segments with artificially large molecular brightness values. Therefore, 2D FIF in essence applies a low-pass filter to the fluorescence images. This inherent low-pass filtering capability of 2D FIF was recently tested by applying 2D FIF on a set of fluorescence images before and after removing high-intensity spots from the images [68]. The relative proportions of the monomer and various oligomer species as a function of concentration remained the same regardless of whether the spot removal procedure was applied to the images.

Two different segmentation methods are used in the 2D FIF approach: the moving square method and the simple linear iterative clustering (SLIC) [69-71] method. In the moving square method, the ROI is bordered by a rectangle that encompasses all vertices of the ROI. This bordering rectangle is broken into a number of smaller segments. Only the pixels which reside within the ROI polygon are included in the calculation of brightness and concentration for a particular segment. In order to avoid including segments with a number of pixels which is insufficient for accurately extracting molecular brightness and concentration, the minimum number of pixels a given segment must contain in order to be used for further analysis is set to be 200 pixels^2. The moving square method has the benefit of executing very quickly. However, because of the need for excluding segments which do not reach the minimum pixel threshold, there are some pixels along the edges of the polygon which end up not being used. The SLIC segmentation method overcomes this drawback inherent to the moving square method by utilizing all pixels contained within the ROI. Initially, the SLIC algorithm breaks an ROI into smaller segment squares of length l_s pixels. The center of mass, (x_i, y_i), of each segment is then calculated. Then, the pixels are reassigned to different segments based on a criterion that takes both pixel location and intensity into account. The center of mass of each segment, which changes as a result of the pixel reassignment, is then recalculated. The pixel reassignment procedure is repeated until the algorithm converges, i.e., pixels are no longer being reassigned to different segments. The drawback to the SLIC segmentation method is that it takes longer to implement than the moving square method.

By scanning a large number of cells, tens of thousands of segments are collected, and an effective brightness and concentration is calculated for each. The molecular brightness, ε, is computed from the background corrected average intensity, $\langle I_s \rangle$, and variance, σ^2, of the measured intensity values in a particular segment, according to the following relation:

$$\varepsilon_{eff} = \frac{\sigma^2 - \sigma_D^2}{\gamma \langle I_s \rangle} \tag{12}$$

where $\varepsilon_{eff} \equiv G\varepsilon$ and G is the analog gain of the fluorescence microscope detector in digital levels /photon. γ is a shape factor which depends on the shape of the laser PSF as well as the geometry of the sample [59]. The variance arising due to the detector, σ_D^2, is subtracted from the total measured variance in order to ensure that the fluctuations in intensity that are quantified are solely due to that of molecules diffusing in and out of the beam. The detector variance can be obtained from separate measurements of a constant intensity light source, where the constant illumination source can be achieved in a number of ways: (i) laser spot scanning the surface of a mirror slide in the plane of focus of the microscope or (ii) turning on a transmitted light illuminator during acquisition. In either case, scans need to be acquired for a range of light intensity levels. Both the variance and mean intensity from small subregions of the scans taken of the constant light source need to be collected and graphed in the form of a scatter plot of the variance vs average intensity. The relationship between the detector variance and intensity is approximately linear, and therefore the scatter plot can be fit with a straight line of slope *S* and intercept σ_o^2. The variance arising due solely to the detector, σ_D^2, is then calculated by the following:

$$\sigma_D^2(\langle I_s \rangle) = \sigma_o^2 + S\langle I_s \rangle \tag{13}$$

The background corrected intensity, $\langle I_s \rangle$, can be obtained for each measurement by subtracting the intensity readout from the detector when there is no sample present, I_{back}, from the total signal readout from the detector in the region of interest, I_{meas}, as follows:

$$I_s = I_{meas} - I_{back} \tag{14}$$

I_{back} can be determined by measuring the mean intensity in multiple regions of the acquisitions where there are no cells/fluorophores present.

The total number of protomers, N_{proto}, can be found from the measured intensity, as follows:

$$N_{proto} = \frac{\langle I_s \rangle}{\varepsilon_{eff}^{proto}}, \tag{15}$$

where $\varepsilon_{eff}^{proto}$ is the molecular brightness of a single protomer. $\varepsilon_{eff}^{proto}$ must be determined from applying eq. (12) to separate measurements on samples expressing a monomeric form of the fluorophore, using the exact same imaging conditions which were used to collect images of cells expressing the fluorescently labeled receptor of interest. The concentration of protomers, *C*, is determined by the following equation:

$$C = \frac{\langle I_s \rangle}{\varepsilon_{eff}^{proto} \mathrm{V}_{PSF}} \tag{16}$$

Here, V_{PSF} is a volume-like quantity calculated by integrating over the point-spread function (PSF) of the focused laser beam:

$$\mathrm{V}_{PSF} = \iiint PSF^{\mathrm{x}}(x, y, \mathrm{z}) dx dy dz \tag{17}$$

The exponent *x* is 2 for single-photon excitation and 4 for two-photon excitation. By assuming a Gaussian-Lorentzian spatial profile for the laser PSF and measuring the e^{-2} laser beam waist at the focal plane (ω_0^2), the volume integral of eq. (17) can be evaluated. It should be noted that V_{PSF} is not a volume in the traditional sense, in that it does not provide definitive boundaries where molecules outside of the volume do not contribute but molecules within the boundary do contribute to the measured signal. The actual volume which encompasses fluorescent proteins contributing to the measured signal will be larger than V_{PSF}. However, due to the non-uniform distribution of the laser intensity, molecules located away from the center of the laser focus contribute less to the measured signal than molecules located at the center. Therefore, to determine the correct concentration of molecules from the measurement of average intensity, $\langle I_s \rangle$, one must account for this non-uniform laser intensity; this is accomplished mathematically by V_{PSF} taking the form in eq. (17).

For fluorescence measurements performed on the basal membranes of cells expressing membrane proteins, we assume that all the fluorescent molecules are bound to the membrane and are together positioned within the focal plane of the laser beam at $z = 0$. Under this condition, the value of the shape factor, γ, needed to calculate ε_{eff} in equation (12) becomes $\gamma = 0.5$. The concentration of the molecules in the membrane, C_m, then becomes the number of molecules per unit area, and is given by:

$$C_m = \frac{\langle I_S \rangle}{\varepsilon_{eff}^{proto} \mathrm{A}_{PSF}} \tag{18}$$

where $\mathrm{A}_{PSF} = \iint PSF^{\mathrm{x}}(x, y, 0)dxdy$. For a Gaussian-Lorentzian PSF, A_{PSF} can be evaluated analytically, with $A_{PSF} = \frac{\pi\omega_0^2}{2}$ for single-photon excitation and $\mathrm{V}_{PSF} = \frac{\pi\omega_0^2}{4}$ for two-photon excitation.

3.3. Deconvolution of molecular brightness distributions to obtain species fraction plots

The collection of brightness and concentration values from each segment in a population of cells is used to assemble a 2D map of all the effective brightness-concentration pairs. From this collection of brightness-concentration pairs, effective brightness distributions, or spectrograms, can be generated for a number of different protomer concentration ranges. Each brightness spectrogram is comprised of contributions from different sized oligomers, and it may be decomposed to find the fraction of total protomers, or relative abundance, present in each of the different sized oligomer species relative to the total number of protomers in the sample.

To extract the species fraction information from each brightness spectrogram, effective brightness values must first be generated from measurements on cells expressing a monomeric form of the fluorescent marker as well as cells expressing a tandem dimer of the fluorescent marker. The monomer and dimer brightness distributions are used as standards from which the brightness distribution for any oligomer of size *n* can be predicted, as the peak value of the brightness distribution from an oligomer of size *n* will be simply scaled by the size of the oligomer relative to the peak of the monomeric distribution. Fitting of the monomer and dimer brightness standards is illustrated in Fig. **4A** and **4B**.

The composite brightness spectrograms are then "unmixed", with the unmixing components consisting of the various predicted oligomer brightness distributions, according to the following equation:

$$S(\varepsilon_{eff}) = \sum_n A_n exp\left[-\frac{\left(\varepsilon_{eff} - n\varepsilon_{eff}^{proto}\right)^2}{2\sigma^2}\right] \tag{19}$$

The mean value of each Gaussian function, $n\varepsilon_{eff}^{proto}$, corresponds to the peak brightness value from a particular oligomer size *n*; these mean values are all linearly related to a multiple of the monomeric molecular brightness. The value of $\varepsilon_{eff}^{proto}$ and σ^2 are determined from the monomeric and dimeric brightness standards, described in the previous paragraph, and held fixed during the fitting. The species fraction for a particular oligomer size is then computed as the fraction of area that its corresponding Gaussian occupies underneath the composite spectrogram:

$$Species\ Fraction_n = \frac{nA_n}{\sum_n nA_n} \tag{20}$$

After unmixing the brightness spectrograms obtained from a number of concentration ranges, the trajectory of the species fraction values obtained for each oligomer size is plotted as a function of concentration. Examples of a deconvoluted brightness spectrogram and species fraction plot are given in Fig. **4C** and **4D**, respectively.

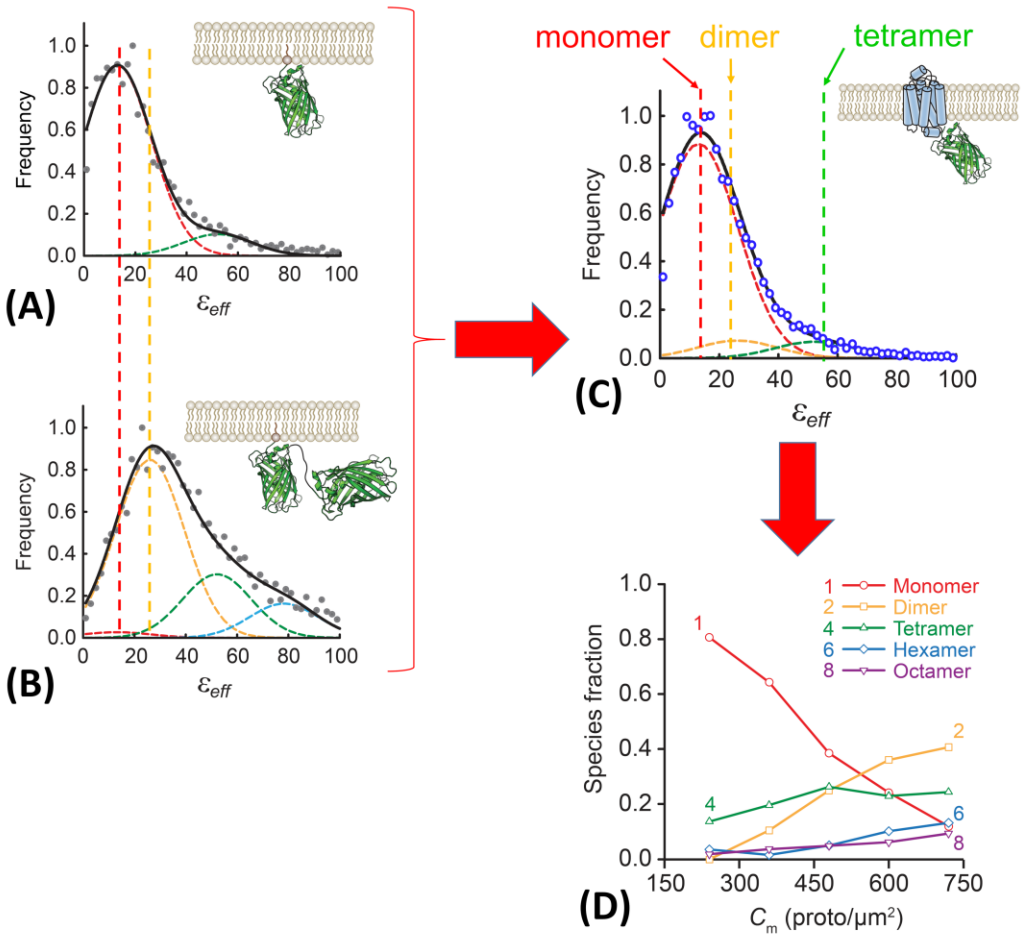

Fig. (4). 2D FIF analysis of ε_{eff} distributions. Figure was adapted from Stoneman *et al.* in Nature Methods 2019 [20] **(A-B)** Normalized frequency distribution assembled from ε_{eff} values obtained from cells expressing plasma membrane-targeted (A) monomeric (PM-1-mEGFP) or (B) tandem dimer (PM-2-mEGFP) mEGFP constructs. The distributions shown in (A) and (B) were simultaneously fitted to a sum (solid black curves) of Gaussians (dashed lines with various colors). Because the molecular brightness of an oligomer complex scales linearly with the size of the oligomer, the means of each of the Gaussians used in the fitting were set equal to the brightness value of a single monomer, $\varepsilon_{eff}^{proto}$, times a multiplicative factor *n*, where *n* represents the size of the oligomer that particular Gaussian corresponds to (e.g., 1, 2, 4, etc.). Therefore, the peak locations of all the Gaussians used in the fitting were dictated by a single parameter, $\varepsilon_{eff}^{proto}$, which was allowed to vary freely during the fitting process. The standard deviations of each of the Gaussians were set equal to a single value, σ, and this value also allowed to vary freely during the fitting. The values of $\varepsilon_{eff}^{proto}$=13.04 and the standard deviations of the Gaussians, σ=13.4, which resulted in the best fit were then used to fit brightness distributions obtained from mEGFP tagged secretin receptors, an example of which is shown in (C). The vertical red and yellow dashed lines indicate positions of $\varepsilon_{eff}^{proto}$ and $2\varepsilon_{eff}^{proto}$, respectively. **(C)** Normalized frequency distribution assembled from ε_{eff} values obtained from cells expressing mEGFP tagged secretin receptors. Only the Gaussian amplitudes (A_n) were adjusted in the process of data fitting; the values of $\varepsilon_{eff}^{proto}$ and σ were held fixed after being determined from the monomeric and dimeric brightness standards shown in (A) and (B). The area underneath the i^{th} Gaussian (relative to the area underneath the entire distribution), $\frac{nA_n}{\sum_n nA_n}$, indicates the fraction of total protomers, or species fraction, that the corresponding oligomeric species comprises. **(D)** Species fraction values for oligomers of size n = 1,2,4,6 and 8 obtained by performing the spectrogram deconvolution procedure shown in (C) for a number of concentration ranges.

3.4. Program for applying 2D FIF

The FIF Spectrometry Suite, a user-friendly software package which is available for download at the following link (https://figshare.com/s/acfd94b21b1105317f56), has been developed for applying 2D FIF to fluorescence images. A commercial version of the suite, which includes a number of additional useful features, is in the final stage of development and testing and will become available in the near future. The entire analysis procedure, from segmenting regions of interest, to calculating brightness and concentration values in each segment, to generating kinetic curves of the relative abundance of various oligomeric species, may be performed using the FIF Spectrometry Suite. The software is broken up into three modules, each of which are responsible for implementing a different part of the FIF analysis. The three modules are entitled: ROI Manager, Fluctuation Data Assembly, and Model Fitting.

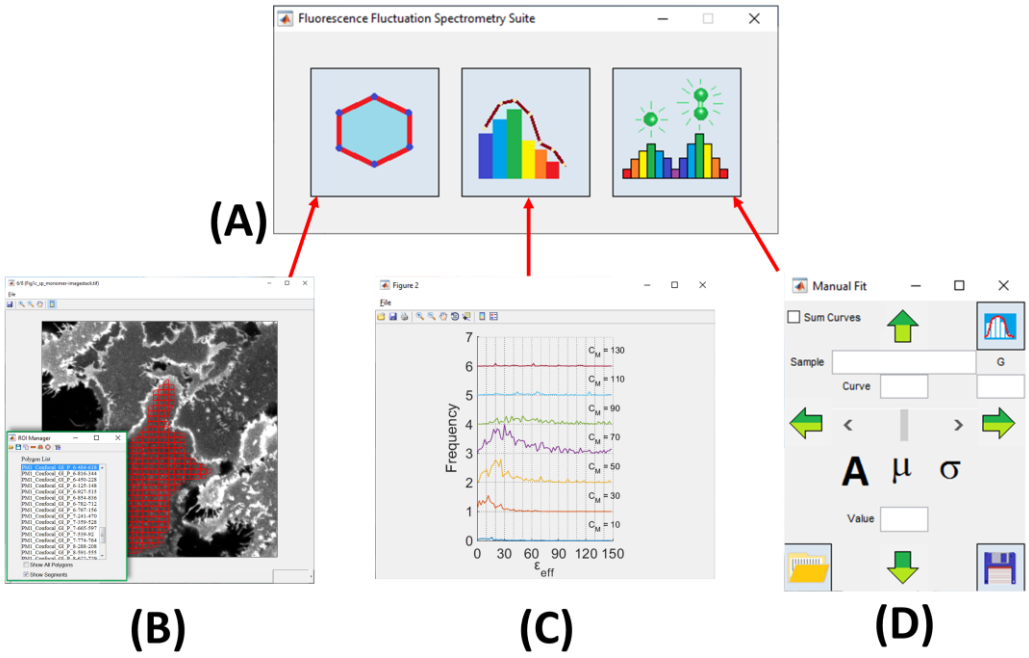

Fig. (5). Various modules of the FIF Spectrometry Suite, a software package for applying 2D FIF to fluorescence images, available for download at the following link (https://figshare.com/s/acfd94b21b1105317f56). **(A)** The Main Toolbar of the FIF Spectrometry Suite, which contains buttons responsible for launching one of the three modules of the suite. Each module is responsible for implementing a different part of the FIF spectrometry analysis. The three modules are entitled: **(B)** ROI Manager, **(C)** Fluctuation Data Assembly, and **(D)** Model Fitting. The main functions of the ROI Manager Module, displayed in (B), include loading a set of fluorescence images, drawing ROI polygons to define the boundaries of entire cells within the images, and segmenting each ROI into smaller regions (segments). The ROI polygons and segments are stored in a list box (located in the ROI manager window) as they are generated; each ROI and corresponding segments can be viewed on the fluorescence image on which it was drawn. The main functions of the Fluctuation Data Assembly Module are to calculate the effective brightness and concentration for each demarcated segment of the fluorescence images, create a two-dimensional surface plot of the frequency of occurrence of each effective brightness-concentration pair, and generate a brightness spectrogram for a number of concentration ranges, as displayed in (C). The Model Fitting Module contains the machinery to fit the effective brightness spectrograms with an array of Gaussian functions using the Fitting window, which is shown in (D).

The main functions of the *ROI Manager Module*, displayed in Fig. **5B**, include the tools to draw ROI polygons on fluorescence images, and segment each ROI into smaller regions (segments). The ROI polygons and segments are stored in a list box (located in the ROI manager window) as they are generated; each ROI and corresponding set of segments can be viewed on the fluorescence image on which it was drawn by simply clicking on the name of the ROI in the list box. The ROI and segment lists can be saved to a file and reloaded at any point using icons located in this module. The demarcated segments are used in the *Fluctuation Data Assembly Module* described below.

The main functions of the *Fluctuation Data Assembly Module* are to calculate the effective brightness and concentration for each demarcated segment of the fluorescence images, create a two-dimensional surface plot of the frequency of occurrence of each effective brightness-concentration pair, and generate a brightness spectrogram for a number of different concentration ranges (displayed in Fig. **5C**). The brightness spectrograms are used for further analysis in the third module, as described below. The brightness and concentration information, as well as any of the generated plots, can be saved to a file and reloaded at any time.

The *Model Fitting Module* contains the tools to fit the effective brightness spectrograms, generated in the *Fluctuation Data Assembly Module*, with an array of Gaussian functions. The mean value of each Gaussian function used in the fitting corresponds to the peak brightness value from a particular oligomer size, and the area of each gaussian (relative to the area underneath the entire spectrogram) reflects the relative abundance of the particular oligomer corresponding to that Gaussian. Each histogram can be fit using the *Fitting Window* (displayed in Fig. **5D**) which is launched from within this module; the *Fitting Window* allows the user to either adjust the parameters of each Gaussian manually, or fit the curve automatically with the push of a button. The species fraction values resulting from the fitting of each spectrogram can be saved to a file in this module.

3.5. Effect of ligand binding on the relative abundances of secretin receptor oligomers as obtained using 2D FIF

Besides being used for evaluating the extent of oligomerization as a function of receptor concentration, as illustrated in Fig. **4**, 2D FIF may also be applied to assess the effects of ligand-inducing shifts in the oligomeric size of membrane receptors of interest. In a recent publication, Stoneman *et al.* [20] investigated the effect of the secretin agonist on the oligomerization properties of the wild type secretin receptor (SecR), a class B GPCR [72]. Cells expressing SecR-mEGFP fusion proteins in their plasma membrane were imaged in the absence and presence of secretin agonist for various incubation times. 2D FIF analysis was applied to the fluorescence images, with the results shown in Fig. **6A-I**. The first observation we can make from inspection of the brightness spectrograms of Fig. **6** is that the spectrograms became broader as the expression levels of SecR increased, both for untreated and ligand-treated cells; this broadening indicates an increase in oligomer size with increasing concentration. Species fraction plots were generated by unmixing the brightness spectrograms generated according to the procedure described in Section 3.3. The species fraction plots confirm the observation of increasing oligomer size as a function of concentration. For the untreated cells, monomers (indicated by the red solid curve in Fig. **6C**) were the most prevalent species at the low expression levels, but decreased in relative abundance as the concentration increased; this decrease in monomer species fraction coincided with an increase in the relative number of protomers forming dimers and tetramers. A similar shift in equilibrium occurred when the cells were treated with ligand. At the lowest concentration, the relative number of monomers decreased to ~0 as the incubation time with secretin increased to 30 minutes. In turn, the number of dimers and tetramers increased with the addition of ligand. At higher concentrations, treatment with ligand appeared to induce the formation of higher order oligomers, as tetramers and octamers started to become prevalent in the species fraction plots.

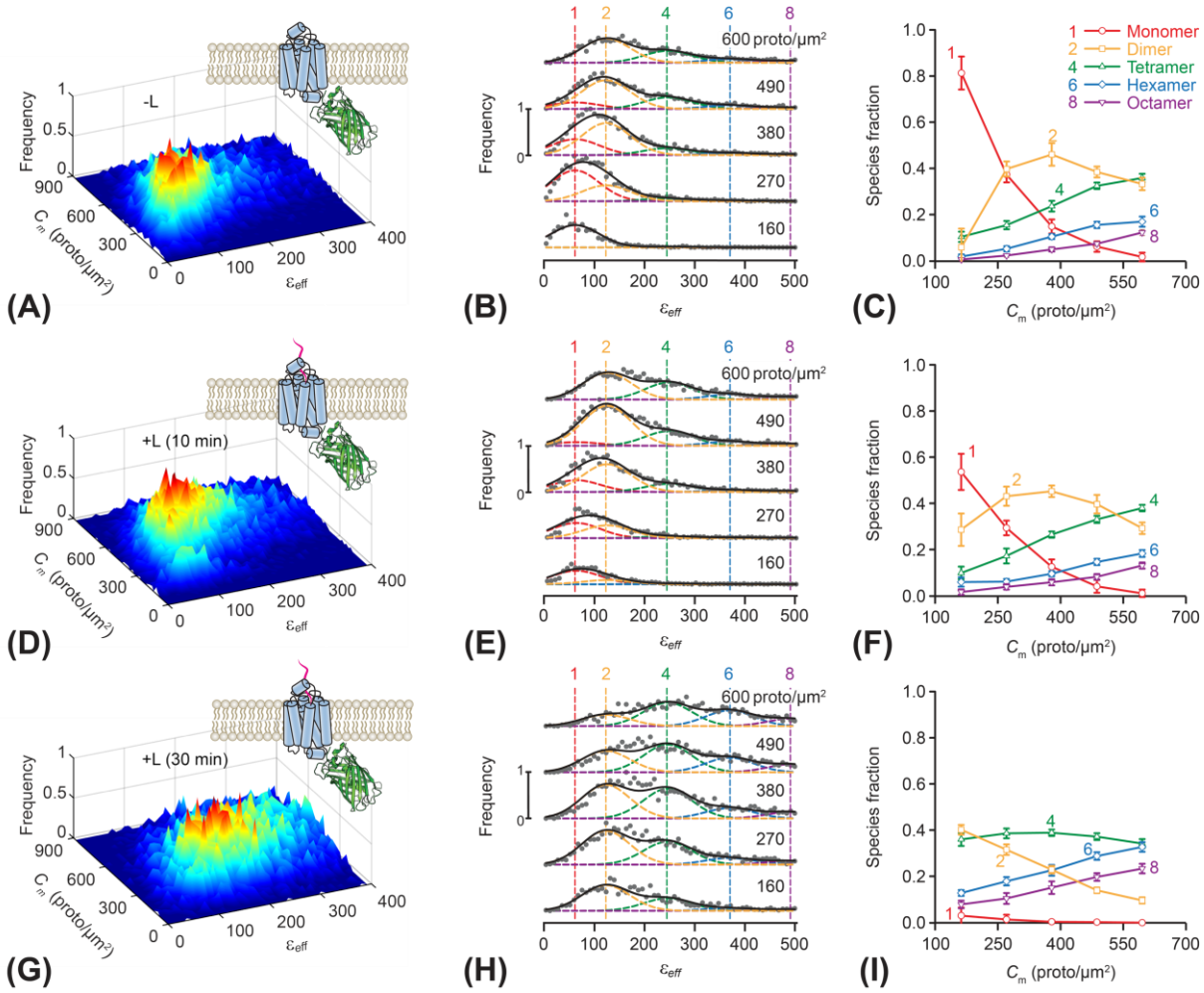

Fig. (6). 2D-FIF results obtained from cells expressing wild-type secretin receptor tagged with mEGFP in the absence of agonist ligand (-L) or after ten- or thirty-minute treatment with 100 nm ligand (+L). Figure was originally published by Stoneman *et al.* in Nature Methods 2019 [20] **(A), (D), (G),** Surface plots of the frequency of occurrence of ε_{eff} for each concentration of protomers. **(B), (E), (H),** Stacks of cross sections through the surface plots in panels **(**A), (D), and (G), respectively, i.e., frequency of occurrence vs. effective brightness for different concentration ranges; the midpoint for each concentration range (in protomer/μm^2) is indicated above each plot. The vertical dashed lines indicate the peak positions for the brightness spectra of monomers, dimers, etc., obtained from (or predicted by) the simultaneous fitting of the monomeric and dimeric constructs used as standards of brightness. **(C), (F), (I),** Relative concentration of protomers within each oligomeric species vs. total concentration of protomers, as derived from unmixing of the curves in (B), (E), and (H), respectively, into different Gaussian components. Samples were as follows: wild-type secretin receptor treated with vehicle (-L) (first row of graphs), secretin (+L) for 10 minutes (second row of graphs), or secretin (+L) for 30 minutes (third row of graphs).

4. CONCLUSION

Discovery of physiologically relevant membrane receptor oligomers has intensified the need for methods to accurately determine protein oligomer states in living cells. Quantifying oligomerization on a receptor-specific basis may yield important insights into the physiological consequences of oligomerization in physiologically normal conditions as well as in disease. Identifying the size and structure of protein oligomers also opens the door for improved pharmacological intervention. For example, designing a potential drug to bind more efficiently to a pair of receptors which are known to be dimeric (or multimeric) could help improve the drug's efficacy and reduce side effects. To this end, reliable methods for probing the association of cellular receptors in cells are needed for a better understanding of

membrane receptor function and for the development of effective therapies that target protein-protein interactions. In this report, we have reviewed two recently developed methods which have proven valuable for providing information on the extent of protein interactions in living cells, FRET Spectrometry and FIF Spectrometry. In FRET Spectrometry, the geometry and stoichiometry of protein oligomers are determined by analyzing pixel level distributions of FRET efficiency with oligomeric models of various quaternary structures. In FIF Spectrometry, spatial fluctuations of protein molecules are analyzed with statistical methods to reveal quantitative information on the size and stability of protein oligomers as a function of receptor concentration. Both methods may be used to study the oligomerization properties of not only GPCRs, but also of other types of cell surface receptors, e.g., enzyme-linked receptors and ligand-gated ion channels, as long as the receptors of interest may be labeled with one or two fluorescent proteins.

The determination of the quaternary structure and interaction strength of protein complexes, which can be obtained by probing the association of cellular receptors with the two methods described in this manuscript, can aid the clinical development of drugs at multiple stages in the drug discovery process, as summarized below. Knowing the strength (i.e., stability) of the interaction is very important at the very start of the drug discovery process for determining whether a particular receptor is a good drug target candidate. This is particularly true in the design of protein-protein interaction inhibitors which are designed to bind to and block the binding interface of the target. Finding a drug which targets the interface of very stable oligomers is a difficult task, because the most probable way to inhibit this type of interaction is to identify compounds that act during protein synthesis. However, it is more feasible to identify compounds which modulate the interactions of more transient complexes. Therefore, information regarding the stability of the interaction, obtainable using the methods described in this paper, is valuable information needed at the start of the drug design process to gauge the "druggability" of a potential target. Once a potential drug target is identified, the experimentally obtained protein quaternary structure can accelerate the design stage of the discovery process. By combining the quaternary structure of the protein complex with the crystal structures of the individual protomers of the oligomer, the binding interfaces, i.e., the surface regions of the proteins which interact with another, between protomers can also be determined. Identification of the amino acids at the protein-protein interface which play the largest role in the intermolecular interaction, and thereby contribute most to the free energy of the interaction, helps streamline the discovery process because potential compounds containing chemical groups that mimic the key contacts made at the protein interaction interface can then be designed. Finally, once an array of potential compounds has been designed and synthesized, resolving the interaction properties, e.g., size and structure, of an oligomer formed by the corresponding drug target greatly enhances the screening of the compounds to determine if they are effective at modifying the interaction properties of said target. A number of clinical assays can indicate whether a potential drug compound binds to the target protein, but do not show whether such binding modifies the interaction. Therefore, quantification of the interaction properties of the protein complex provides useful insight for assessing the efficacy of the potential compound.

One promising area of development with regard to the two techniques presented in this manuscript would be to combine them such that they are "simultaneously" applied to the same fluorescence images. FRET spectrometry is ideally suited to measure intramolecular distances between protein subunits in a complex, and hence it can deliver information on the proteins quaternary structure. However, this method can be time-intensive because of a lengthy analysis procedure which includes the fitting of many types of oligomer size and shape models, which sometimes can give inconclusive results due to multiple models fitting the data equally well. Conversely, FIF spectrometry extracts information on the average receptor oligomer size but does not provide any information on the quaternary structure. Therefore, FIF adds valuable complementary information to FRET spectrometry, in that it can reduce the number of models needed to be tested. It has been proposed that these techniques could be further refined and potentially merged in order to simplify the experimental protocol for extraction of concentration and energy transfer information simultaneously [73, 74]. The combination of the methods of FIF and FRET spectrometry would allow for not only the extraction of equilibrium association/dissociation constants characterizing the equilibrium between oligomeric species, but also the determination of the inter-protomer distances within the oligomers. Changes in the equilibrium constants and/or inter-protomer distances of the oligomers may then be probed after treating the receptors with various agonists, antagonists, and inverse agonists. While it has been demonstrated that some, or all, of this information is attainable using either FIF or FRET spectrometry on their own, the combination of the two improve the resolution with which equilibrium constants and the inter-protomer distances of the protein complexes are determined, because simultaneously analyzing the two sets of complementary data help reduce ambiguity in the data fitting procedures.

Furthermore, the enhancement in efficiency of the analysis routine would in turn increase the throughput at which this information could be obtained, as the same fluorescence images are analyzed with both techniques, and therefore no increase in data acquisition time is needed to combine the two. The enhanced resolution by which the quaternary structure and strength of interaction of the protein complex can be determined and increase in throughput obtained from a combination of FRET and FIF spectrometry would make these techniques even more valuable in the area of characterizing membrane receptor oligomers for structure-based drug design.

CONSENT FOR PUBLICATION

Not applicable.

FUNDING

This work was partly supported by grants from the National Science Foundation (grant numbers PHY-1126386 and DBI-1919670) as well as the UWM Research Growth Initiative (101X396) awarded to V.R.

CONFLICT OF INTEREST

The authors declare no conflict of interest, financial or otherwise.

ACKNOWLEDGEMENTS

Declared none.

REFRENCES

[1] Rosenbaum DM, Rasmussen SG, Kobilka BK. The structure and function of G-protein-coupled receptors. Nature 2009; 459: 356-63.

[2] Venkatakrishnan AJ, Deupi X, Lebon G, Tate CG, Schertler GF, Babu MM. Molecular signatures of G-protein-coupled receptors. Nature 2013; 494: 185-194.

[3] Milligan G. The Prevalence, Maintenance, and Relevance of G Protein-Coupled Receptor Oligomerization. Mol Pharmacol 2013; 84: 158-169.

[4] Lagerstrom MC, Schioth HB. Structural diversity of G protein-coupled receptors and significance for drug discovery. Nat Rev Drug Discov 2008; 7: 339-357.

[5] Palczewski K. Oligomeric forms of G protein-coupled receptors (GPCRs). Trends Biochem Sci 2010; 35: 595-600.

[6] Farran B. An update on the physiological and therapeutic relevance of GPCR oligomers. Pharmacol Res 2017; 117: 303-327.

[7] Park PSH, Wells JW. Monomers and oligomers of the M-2 muscarinic cholinergic receptor purified from Sf9 cells. Biochemistry 2003; 42: 12960-12971.

[8] Milligan G. G protein-coupled receptor hetero-dimerization: contribution to pharmacology and function. Br J Pharmacol 2009; 158: 5-14.

[9] Patowary S, Alvarez-Curto E, Xu TR*, et al.* The Muscarinic M3 Acetylcholine receptor exists as two differently sized complexes at the plasma membrane. Biochem J 2013; 452: 303-312.

[10] Raicu V, Stoneman MR, Fung R*, et al.* Determination of supramolecular structure and spatial distribution of protein complexes in living cells. Nat Photonics 2009; 3: 107-113.

[11] Ferre S. The GPCR heterotetramer: challenging classical pharmacology. Trends Pharmacol Sci 2015; 36: 145-152.

[12] Overton MC, Chinault SL, Blumer KJ. Oligomerization of G-protein-coupled receptors: Lessons from the yeast Saccharomyces cerevisiae. Eukaryot Cell 2005; 4: 1963-1970.

[13] Maurel D, Comps-Agrar L, Brock C*, et al.* Cell-surface protein-protein interaction analysis with time-resolved FRET and snap-tag technologies: application to GPCR oligomerization. Nat Methods 2008; 5: 561-7.

[14] Lundstrom K. An overview on GPCRs and drug discovery: structure-based drug design and structural biology on GPCRs. Methods Mol Biol 2009; 552: 51-66.
[15] Anderson AC. The process of structure-based drug design. Chem Biol 2003; 10: 787-797.
[16] Dalrymple MB, Pfleger KDG, Eidne KA. G protein-coupled receptor dimers: Functional consequences, disease states and drug targets. Pharmacol Ther 2008; 118: 359-371.
[17] Panetta R, Greenwood MT. Physiological relevance of GPCR oligomerization and its impact on drug discovery. Drug Discov Today 2008; 13: 1059-1066.
[18] Glass M, Govindpani K, Furkert DP, Hurst DP, Reggio PH, Flanagan JU. One for the Price of Two...Are Bivalent Ligands Targeting Cannabinoid Receptor Dimers Capable of Simultaneously Binding to both Receptors? Trends Pharmacol Sci 2016; 37: 353-363.
[19] Carli M, Kolachalam S, Aringhieri S*, et al.* Dopamine D-2 Receptors Dimers: How can we Pharmacologically Target Them? Curr Neuropharmacol 2018; 16: 222-230.
[20] Stoneman MR, Biener G, Ward RJ*, et al.* A general method to quantify ligand-driven oligomerization from fluorescence-based images. Nat Methods 2019; 16: 493-496.
[21] Milligan G, Ward RJ, Marsango S. GPCR homo-oligomerization. Curr Opin Cell Biol 2019; 57: 40-47.
[22] Raicu V, Singh DR. FRET Spectrometry: A New Tool for the Determination of Protein Quaternary Structure in Living Cells. Biophys J 2013; 105: 1937-1945.
[23] Selvin PR. The renaissance of fluorescence resonance energy transfer. Nat Struct Mol Biol 2000; 7: 730-4.
[24] Förster T. Zwischenmolekulare Energiewanderung und Fluoreszenz. Annalen der Physik 1948; 2: 55-75.
[25] Clegg RM. Fluorescence resonance energy transfer. In: X.F. Wang and B. Herman, Eds. Fluorescence Imaging Spectroscopy and Microscopy. New York: Wiley 1996; pp. 179-252.
[26] King C, Stoneman M, Raicu V, Hristova K. Fully quantified spectral imaging reveals in vivo membrane protein interactions. Integrative Biology 2016; 8: 216-229.
[27] Chen LR, Novicky L, Merzlyakov M, Hristov T, Hristova K. Measuring the Energetics of Membrane Protein Dimerization in Mammalian Membranes. J Am Chem Soc 2010; 132: 3628-3635.
[28] Singh DR, Kanvinde P, King C, Pasquale EB, Hristova K. The EphA2 receptor is activated through induction of distinct, ligand-dependent oligomeric structures. Communications Biology 2018; 1: 1-12.
[29] Albizu L, Cottet M, Kralikova M*, et al.* Time-resolved FRET between GPCR ligands reveals oligomers in native tissues. Nat Chem Biol 2010; 6: 587-594.
[30] King C, Wirth D, Workman S, Hristova K. Interactions between NRP1 and VEGFR2 molecules in the plasma membrane. Biochimica Et Biophysica Acta-Biomembranes 2018; 1860: 2118-2125.
[31] King C, Hristova K. Direct measurements of VEGF-VEGFR2 binding affinities reveal the coupling between ligand binding and receptor dimerization. J Biol Chem 2019; 294: 9064-9075.
[32] Mishra AK, Gragg M, Stoneman MR*, et al.* Quaternary structures of opsin in live cells revealed by FRET spectrometry. Biochem J 2016; 473: 3819-3836.
[33] Schmidt S, Jakab M, Costa I*, et al.* Quaternary Structure Assessment of ICln by Fluorescence Resonance Energy Transfer (FRET) in vivo. Cell Physiol Biochem 2009; 23: 397-406.

[34] Demarco IA, Periasamy A, Booker CF, Day RN. Monitoring dynamic protein interactions with photoquenching FRET. Nat Methods 2006; 3: 519-524.
[35] Ferrari ML, Gomez GA, Maccioni HJF. Spatial Organization and Stoichiometry of N-Terminal Domain-Mediated Glycosyltransferase Complexes in Golgi Membranes Determined by Fret Microscopy. Neurochem Res 2012; 37: 1325-1334.
[36] Hochreiter B, Kunze M, Moser B, Schmid JA. Advanced FRET normalization allows quantitative analysis of protein interactions including stoichiometries and relative affinities in living cells. Sci Rep 2019; 9.
[37] Raicu V, Jansma DB, Miller RJ, Friesen JD. Protein interaction quantified in vivo by spectrally resolved fluorescence resonance energy transfer. Biochem J 2005; 385: 265-77.
[38] Stoneman MR, Paprocki JD, Biener G*, et al.* Quaternary structure of the yeast pheromone receptor Ste2 in living cells. Biochimica Et Biophysica Acta-Biomembranes 2017; 1859: 1456-1464.
[39] Li M, Reddy LG, Bennett R, Silva ND, Jones LR, Thomas DD. A fluorescence energy transfer method for analyzing protein oligomeric structure: Application to phospholamban. Biophys J 1999; 76: 2587-2599.
[40] Woehler A, Wlodarczyk J, Ponimaskin EG. Specific oligomerization of the 5-HT1A receptor in the plasma membrane. Glycoconj J 2009; 26: 749-756.
[41] King C, Raicu V, Hristova K. Understanding the FRET Signatures of Interacting Membrane Proteins. J Biol Chem 2017; 292: 5291-5310.
[42] Raicu V. Ab Initio Derivation of the FRET Equations Resolves Old Puzzles and Suggests Measurement Strategies. Biophys J 2019; 116: 1313-1327.
[43] Raicu V. Efficiency of resonance energy transfer in homo-oligomeric complexes of proteins. J Biol Phys 2007; 33: 109-127.
[44] Singh DR, Mohammad MM, Patowary S*, et al.* Determination of the quaternary structure of a bacterial ATP-binding cassette (ABC) transporter in living cells. Integrative Biology 2013; 5: 312-323.
[45] Harikumar KG, Miller LJ. Monitoring the State of Cholecystokinin Receptor Oligomerization after Ligand Binding Using Decay of Time-Resolved Fluorescence Anisotropy. Ann Ny Acad Sci 2008; 1144: 21-27.
[46] Ward RJ, Pediani JD, Godin AG, Milligan G. Regulation of oligomeric organization of the serotonin 5-hydroxytryptamine 2C (5-HT2C) receptor observed by spatial intensity distribution analysis. J Biol Chem 2015; 290: 12844-57.
[47] Godin AG, Costantino S, Lorenzo LE*, et al.* Revealing protein oligomerization and densities in situ using spatial intensity distribution analysis. Proc Natl Acad Sci U S A 2011; 108: 7010-7015.
[48] Raicu V, Schmidt WF. Advanced Microscopy Techniques. In: K. Herrick-Davis, G. Milligan, and G. Di Giovanni, Eds. G-Protein-Coupled Receptor Dimers. New York: Humana Press 2017; pp. 39-75.
[49] Sinclair MB, Haaland DM, Timlin JA, Jones HDT. Hyperspectral confocal microscope. Applied Optics 2006; 45: 6283-6291.
[50] Raicu V, Fung R, Melnichuck M, Chaturvedi A, Gillman D. Combined spectrally-resolved multiphoton microscopy and transmission microscopy employing a high-sensitivity electron-multiplying CCD camera. Multiphoton Microscopy in the Biomedical Sciences VII. 2007; Proc. SPIE 6442: 64420M.

[51] Zhang ZY, Kenny SJ, Hauser M, Li W, Xu K. Ultrahigh-throughput single-molecule spectroscopy and spectrally resolved super-resolution microscopy. Nat Methods 2015; 12: 935-938.
[52] Biener G, Stoneman MR, Acbas G*, et al.* Development and Experimental Testing of an Optical Micro-Spectroscopic Technique Incorporating True Line-Scan Excitation. Int J Mol Sci 2014; 15: 261-276.
[53] Elliott AD, Gao L, Ustione A*, et al.* Real-time hyperspectral fluorescence imaging of pancreatic beta-cell dynamics with the image mapping spectrometer. J Cell Sci 2012; 125: 4833-4840.
[54] Lavagnino Z, Dwight J, Ustione A, Nguyen TU, Tkaczyk TS, Piston DW. Snapshot Hyperspectral Light-Sheet Imaging of Signal Transduction in Live Pancreatic Islets. Biophys J 2016; 111: 409-417.
[55] Neher R, Neher E. Optimizing imaging parameters for the separation of multiple labels in a fluorescence image. J Microsc 2004; 213: 46-62.
[56] Thaler C, Koushik SV, Blank PS, Vogel SS. Quantitative multiphoton spectral imaging and its use for measuring resonance energy transfer. Biophys J 2005; 89: 2736-2749.
[57] Zimmermann T, Rietdorf J, Girod A, Georget V, Pepperkok R. Spectral imaging and linear un-mixing enables improved FRET efficiency with a novel GFP2-YFP FRET pair. FEBS Lett 2002; 531: 245-249.
[58] Mishra AK, Mavlyutov T, Singh DR*, et al.* The sigma-1 receptors are present in monomeric and oligomeric forms in living cells in the presence and absence of ligands. Biochem J 2015; 466: 263-71.
[59] Chen Y, Muller JD, So PT, Gratton E. The photon counting histogram in fluorescence fluctuation spectroscopy. Biophys J 1999; 77: 553-67.
[60] Herrick-Davis K, Grinde E, Cowan A, Mazurkiewicz JE. Fluorescence Correlation Spectroscopy Analysis of Serotonin, Adrenergic, Muscarinic, and Dopamine Receptor Dimerization: The Oligomer Number Puzzle. Mol Pharmacol 2013; 84: 630-642.
[61] Digman MA, Dalal R, Horwitz AF, Gratton E. Mapping the number of molecules and brightness in the laser scanning microscope. Biophys J 2008; 94: 2320-32.
[62] Unruh JR, Gratton E. Analysis of molecular concentration and brightness from fluorescence fluctuation data with an electron multiplied CCD camera. Biophys J 2008; 95: 5385-98.
[63] Nagy P, Claus J, Jovin TM, Arndt-Jovin DJ. Distribution of resting and ligand-bound ErbB1 and ErbB2 receptor tyrosine kinases in living cells using number and brightness analysis. Proc Natl Acad Sci U S A 2010; 107: 16524-16529.
[64] Pediani JD, Ward RJ, Marsango S, Milligan G. Spatial Intensity Distribution Analysis: Studies of G Protein-Coupled Receptor Oligomerisation. Trends Pharmacol Sci 2018; 39: 175-186.
[65] Digman MA, Wiseman PW, Choi C, Horwitz AR, Gratton E. Stoichiometry of molecular complexes at adhesions in living cells. Proc Natl Acad Sci U S A 2009; 106: 2170-2175.
[66] Godin AG, Rappaz B, Potvin-Trottier L, Kennedy TE, De Koninck Y, Wisemant PW. Spatial Intensity Distribution Analysis Reveals Abnormal Oligomerization of Proteins in Single Cells. Biophys J 2015; 109: 710-721.
[67] Chen Y, Wei LN, Muller JD. Probing protein oligomerization in living cells with fluorescence fluctuation spectroscopy. Proc Natl Acad Sci U S A 2003; 100: 15492-15497.

[68] Stoneman MR, Biener G, Raicu V. Reply to: Spatial heterogeneity in molecular brightness. Nat Methods 2020; 17: 276-278.
[69] Achanta R, Shaji A, Smith K, Lucchi A, Fua P, Susstrunk S. SLIC Superpixels Compared to State-of-the-Art Superpixel Methods. Ieee Transactions on Pattern Analysis and Machine Intelligence 2012; 34: 2274-2281.
[70] Achanta R, Shaji A, Smith K, Luchhi A, Fua P, Susstrunk S. SLIC Superpixels. EPFL Technical Report 2010; 149300,1-15.
[71] Zhang YX, Li XM, Gao XF, Zhang CM. A Simple Algorithm of Superpixel Segmentation With Boundary Constraint. Ieee Transactions on Circuits and Systems for Video Technology 2017; 27: 1502-1514.
[72] Miller LJ, Dong MQ, Harikumar KG. Ligand binding and activation of the secretin receptor, a prototypic family B G protein-coupled receptor. Br J Pharmacol 2012; 166: 18-26.
[73] Raicu V. Extraction of information on macromolecular interactions from fluorescence micro-spectroscopy measurements in the presence and absence of FRET. Spectrochimica Acta Part a-Molecular and Biomolecular Spectroscopy 2018; 199: 340-348.
[74] Stoneman MR, Biener G, Raicu V. Proposal for simultaneous analysis of fluorescence intensity fluctuations and resonance energy transfer (IFRET) measurements. Methods Appl Fluores 2020; 8: 035011.